Research Square

Preprints are preliminary reports that have not undergone peer review.
They should not be considered conclusive, used to inform clinical practice,
or referenced by the media as validated information.

KLF5-Mediated Transcriptional Repression of PGC-1α Impairs Fatty Acid Oxidation and Aggravates Sepsis- Associated Acute Kidney Injury

Jing Liu
The First Affiliated Hospital of Harbin Medical University
Yingyue Ding
The First Affiliated Hospital of Harbin Medical University
Pengzhan Liu
The First Affiliated Hospital of Harbin Medical University
Mingyu xu
The First Affiliated Hospital of Harbin Medical University
Wuyang Lv
The First Affiliated Hospital of Harbin Medical University
Yingying Zhai
The First Affiliated Hospital of Harbin Medical University
Wenze Hou
The First Affiliated Hospital of Harbin Medical University
Yingyu Jin
jyyharbin@163.com

The First Affiliated Hospital of Harbin Medical University

Research Article

Keywords: Sepsis-associated acute kidney injury, KLF5, Fatty acid oxidation, Inflammation, lipopolysaccharide (LPS), Peroxisome proliferator-activated receptor gamma coactivator 1-alpha (PGC-1α)(PPARGC1A), KLF, Transcription regulation, Lipid metabolic disorder

Posted Date: September 24th, 2026

DOI: https://doi.org/10.21203/rs.3.rs-10921398/v1

License: This work is licensed under a Creative Commons Attribution 4.0 International License.
Read Full License

Additional Declarations: No competing interests reported.

Abstract

Sepsis-associated acute kidney injury (SA-AKI) is a common life-threatening complication in critically ill patients, yet the upstream mechanisms underlying tubular fatty acid oxidation (FAO) dysfunction remain unclear. Here, we identify a previously unrecognized role of Krüppel-like factor 5 (KLF5) in SA-AKI. Serum KLF5 was significantly elevated in SA-AKI patients. Transcriptome sequencing of renal tissues from LPS-induced SA-AKI rats at 3, 6, and 12 h revealed a negative correlation between *Klf5* and key FAO genes. Using dual-luciferase reporter assays and gene knockdown experiments in HK-2 cells, we demonstrate for the first time that KLF5 directly binds the *PPARGC1A* (PGC-1α) promoter and transcriptionally represses its expression, leading to downregulation of PPARα and CPT1A, impaired FAO, reduced ATP production, and lipid accumulation, thereby aggravating tubular injury. Both pharmacological inhibition of KLF5 by ML264 in vivo and siRNA-mediated KLF5 knockdown in vitro reversed these metabolic disturbances and alleviated renal injury. These findings establish the KLF5–PGC-1α–FAO axis as a novel pathogenic mechanism and identify KLF5 as a promising therapeutic target for metabolic intervention in SA-AKI.

1. Introduction

SA-AKI represents one of the most life-threatening complications in critically ill patients[1, 2]. According to the consensus of the Acute Disease Quality Initiative (ADQI), SA-AKI is defined as acute kidney injury that develops within seven days of sepsis onset and meets the diagnostic criteria established by the Kidney Disease: Improving Global Outcomes (KDIGO) working group. Epidemiological evidence indicates that nearly half of patients with sepsis develop SA-AKI, with an in-hospital mortality rate exceeding 50%. Moreover, surviving patients face a markedly elevated long-term risk of progressing to chronic kidney disease (CKD) and end-stage renal disease (ESRD) [3]. Currently, clinical management of SA-AKI is limited to supportive interventions, including fluid resuscitation and anti-infective therapy, and no targeted therapeutic agents are available [4, 5]. Therefore, further exploration of the pathological mechanisms underlying SA-AKI progression is urgently required to identify effective therapeutic targets.

Renal proximal tubular epithelial cells (PTECs) consume large amounts of energy to sustain physiological functions such as tubular reabsorption and substance transport. Under physiological conditions, mitochondrial FAO serves as the primary energy source for PTECs, generating sufficient ATP to maintain cellular viability and renal homeostasis [6–8]. Nevertheless, septic inflammatory stress impairs tubular FAO, resulting in severe cellular energy deficit. Impaired FAO further restricts ATP synthesis and causes excessive intracellular lipid accumulation, subsequently inducing lipotoxic injury, mitochondrial dysfunction, and progressive tubular damage [9]. Accumulating evidence suggests that restoring endogenous FAO activity effectively attenuates renal injury, and FAO suppression is widely recognized as a core pathogenic driver of SA-AKI[10].

KLF5, a zinc-finger transcription factor, modulates multiple biological processes including cell proliferation, apoptosis, and inflammatory responses. Dysregulated KLF5 expression is closely

implicated in tissue fibrosis and tumor progression [11, 12]. Studies in oncology have demonstrated that KLF5 upregulates fatty acid synthase (FASN) to promote lipid synthesis and remodel lipid metabolism in lung cancer [13]. In multiple renal injury models, including unilateral ureteral obstruction, subtotal nephrectomy, and diabetic nephropathy, as well as during human kidney injury after kidney transplantation, tubular KLF5 expression is significantly elevated, thereby exacerbating renal damage and fibrosis; conversely, *Klf5* knockout effectively ameliorates renal pathological changes [14–17]. Importantly, recent studies have confirmed marked upregulation of KLF5 in the kidneys of septic mice [18, 19]. Although the regulatory role of KLF5 in tumor lipid reprogramming has been documented, its functional effect on tubular FAO during septic renal injury remains uncharacterized.

Peroxisome proliferator-activated receptor gamma coactivator-1α (PGC-1α) is a core transcriptional regulator of mitochondrial biogenesis and fatty acid catabolism[20, 21]. Activated PGC-1α initiates transcription of a broad spectrum of FAO-related genes. As a key downstream target of PGC-1α, peroxisome proliferator-activated receptor α (PPARα) serves as a nuclear transcription factor that triggers the FAO transcriptional program. Carnitine palmitoyltransferase 1A (CPT1A), the rate-limiting enzyme of FAO, mediates the transmembrane transport of fatty acids into mitochondria for β-oxidation[22–24]. The combined expression levels of PPARα and CPT1A directly reflect the overall FAO efficiency of renal tubular cells. Previous studies have demonstrated that PGC-1α activation reverses metabolic disorders in injured renal tissues[25, 26]. Mounting evidence indicates that septic stress induces simultaneous reductions in PGC-1α expression and FAO activity in renal tubules [9, 27]. However, it remains unclear whether sepsis-induced KLF5 upregulation disrupts FAO homeostasis and exacerbates SA-AKI by transcriptionally inhibiting PGC-1α and subsequently downregulating PPARα and CPT1A expression. In the present study, an in vivo LPS-induced SA-AKI rat model and an in vitro HK-2 tubular injury model were established. We systematically assessed renal function, pathological lesions, intracellular ATP content, lipid deposition, and the expression profiles of KLF5, PGC-1α, PPARα, and CPT1A. This study aims to elucidate the pathogenic regulatory role of the KLF5-PGC-1α-FAO signaling axis in LPS-triggered SA-AKI, thereby providing novel experimental evidence and potential therapeutic targets for clinical management of SA-AKI.

2. Experimental procedures

2.1 Transcriptome Sequencing Analysis

Male Wistar rats were randomly divided into four experimental groups: blank control group (n = 4), LPS 3 h intervention group (n = 5), LPS 6 h intervention group (n = 5), and LPS 12 h intervention group (n = 5). After LPS treatment for the corresponding durations, renal tissues were harvested and preserved in RNA stabilization solution. Total tissue RNA was extracted for high-throughput transcriptome sequencing. RStudio software was used to screen differentially expressed genes (DEGs) between LPS-treated groups and the control group. Gene Ontology (GO) functional annotation and Kyoto Encyclopedia of Genes and Genomes (KEGG) pathway enrichment analyses were subsequently performed to characterize the functional properties of identified DEGs.

2.2 Animal Model Establishment Animal Model Establishment

Male Wistar rats aged 6–8 weeks with body weights of 180–220 g were obtained from the Beijing Vital River Laboratory Animal Technology. All rats were housed in a specific pathogen-free (SPF) environment with a constant temperature of 22 ± 2 ℃ and free access to standard chow and sterile water. A 7-day adaptive feeding period was implemented before formal experiments. After adaptive feeding, rats were randomly assigned to four groups: blank control group (n = 8), LPS model group (n = 8), ML264 single-treatment group (n = 4), and ML264 + LPS combined intervention group (n = 4). Fresh LPS solution was prepared with sterile 0.9% normal saline, and SA-AKI was induced via a single intraperitoneal injection of LPS at a dose of 10 mg/kg. The blank control group received an equal volume of sterile normal saline at the corresponding time point. All rats were maintained under consistent feeding conditions throughout the experiment. All animals were euthanized 12 h after LPS administration, and renal tissues were rapidly isolated with redundant peripheral tissues removed. Left renal tissues were frozen and stored at − 80 ℃ for subsequent molecular biomarker detection, while right renal tissues were fixed in 4% paraformaldehyde for histological analysis.

2.3 Renal Function Detection

Cardiac blood samples were collected 12 h after LPS intervention. After room-temperature coagulation, serum was separated via centrifugation at 3000 rpm for 10 min. Serum creatinine (Scr) and blood urea nitrogen (BUN) levels were measured using matched detection kits on an automatic biochemical analyzer. Successful establishment of the SA-AKI model was defined as a ≥ 1.5-fold increase in Scr levels in the LPS group relative to the blank control group.

2.4 Hematoxylin-Eosin (H&E) Staining

Renal tissues were fixed in 4% paraformaldehyde for 24 h, embedded in paraffin, and cut into continuous 4-μm sections. Conventional H&E staining was performed using a commercial staining kit, and histopathological morphological changes in renal tissues were observed and photographed under an optical microscope.

2.5 Immunohistochemical Staining

Paraffin-embedded renal sections were deparaffinized and rehydrated, followed by antigen retrieval using citrate buffer (pH 6.0). After blocking non-specific binding sites, sections were incubated with primary antibodies against KLF5, CPT1A, and PPARα overnight at 4 ℃. On the next day, sections were incubated with HRP-conjugated secondary antibodies. Staining was developed using a DAB chromogenic kit, followed by hematoxylin counterstaining, mounting, and microscopic observation. Multiple non-overlapping visual fields were randomly selected for each section, and the positive staining area percentage (% Area) was quantitatively analyzed using ImageJ software.

2.6 Immunofluorescence Staining

Renal paraffin sections were deparaffinized, rehydrated, and subjected to antigen retrieval with citrate buffer (pH 6.0). Sections were permeabilized with 0.1% Triton X-100 and blocked with BSA blocking solution at room temperature. Subsequently, sections were incubated with primary antibodies targeting KLF5, CPT1A, and PPARα overnight at 4 ℃. After incubation with corresponding fluorescent secondary antibodies in the dark, cell nuclei were stained with DAPI. Sections were mounted, and fluorescent images were captured using a laser confocal microscope.

2.7 Oil Red O Staining

Lipid accumulation in renal tissues and HK-2 cells was detected via Oil Red O staining. Renal tissues were embedded in OCT compound and cut into 10 μm frozen sections. After fixation and pretreatment with 60% isopropanol, sections were stained with freshly prepared Oil Red O working solution, differentiated with 60% isopropanol, washed with distilled water, counterstained with hematoxylin, and mounted with water-soluble mounting medium. Fixed HK-2 cells were stained following the identical procedure. Multiple non-overlapping fields were randomly captured under an optical microscope, and the percentage of lipid-positive areas was quantified using ImageJ software.

2.8 Transmission Electron Microscopy

Fresh renal cortex tissues were harvested and immediately cut into 1 mm^3 pieces on ice. Specimens were fixed in 2.5% glutaraldehyde diluted in 0.05 M sodium cacodylate buffer (pH 7.2) at 25°C for 2 h. After buffer rinsing, samples were post-fixed with 2% OsO_4 in 0.1 M sodium cacodylate buffer for 2 h, and then stained en bloc with 1% aqueous uranyl acetate at 4°C for 18 h. Subsequently, tissues were dehydrated through a graded series of ethanol solutions, infiltrated, and embedded in epoxy resin 618 at 40°C. Ultrathin sections with a thickness of 60–80 nm were cut using an ultramicrotome, followed by double staining with uranyl acetate and lead citrate at 4°C for 20 min. The ultrastructural morphology of mitochondria and lipid droplets in renal tubular epithelial cells was observed and photographed under a transmission electron microscope.

2.9 Cell Culture and Treatment

Human renal tubular epithelial HK-2 cells were cultured in complete medium supplemented with 10% fetal bovine serum (FBS) and 1% penicillin-streptomycin double antibiotics, in a humidified incubator with 5% CO_2 at 37 ℃. Cells were passaged when reaching 70%–80% confluence, and low-passage cells were used for all in vitro experiments. An in vitro SA-AKI cell injury model was constructed by stimulating HK-2 cells with LPS.

2.10 Cell Transfection

Transient transfection was performed when HK-2 cells reached 70%–80% confluence. Three small interfering RNA (siRNA) sequences targeting KLF5 (siKLF5-1, siKLF5-2, siKLF5-3), three siRNA sequences targeting PGC-1α (siPGC-1α-1, siPGC-1α-2, siPGC-1α-3), and negative control siRNA were synthesized for this experiment. siRNA and commercial transfection reagents were diluted in serum-free medium to prepare transfection complexes, which were added to cell culture medium after room-

temperature incubation. After routine culture post-transfection, cells were treated with LPS to establish the in vitro SA-AKI model for subsequent functional detection.

2.11 Biochemical Detection

Rat serum samples and HK-2 cell lysate supernatants were collected for biochemical detection. Triglyceride (TG) and non-esterified fatty acid (NEFA) levels were measured using matched commercial kits via the rate method on an automatic biochemical analyzer at 37 ℃.

2.12 Western Blotting Analysis

Total proteins were extracted from rat renal cortex tissues and HK-2 cells using RIPA lysis buffer supplemented with a protease inhibitor cocktail on ice. After centrifugation, supernatant protein samples were mixed with loading buffer and denatured by boiling. Proteins were separated via SDS-PAGE electrophoresis and transferred to PVDF membranes, followed by 10-minute blocking with rapid room-temperature blocking solution. Membranes were incubated with primary antibodies overnight at 4 ℃, including KLF5 (21017-1-AP, 1:7000, Proteintech, China), PGC-1α (A11971, 1:1000, Abclonal, China), CPT1A (15184-1-AP, 1:7000, Proteintech, China), PPARα (WL00978, 1:1000, Wanlei, China), KIM-1 (CY8586, 1:1000, Abways, China), IL-6 (WL02841, 1:1000, Abmart, China), IL-1β (TA5103, 1:1000, Abmart, China), TNF-α (PY19810, 1:1000, Abmart, China), NGAL (CY6730, 1:1000, Abways, China), and β-actin (81115-1-RR, 1:8000, Proteintech, China). After thorough washing with TBST, membranes were incubated with HRP-conjugated secondary antibodies at room temperature for 1 h. Protein bands were visualized using enhanced chemiluminescence (ECL) reagent. Band gray values were quantified with ImageJ software and normalized to the internal reference β-actin for relative quantitative analysis.

2.13 Quantitative Real-Time PCR (qRT-PCR)

Total RNA was extracted from rat renal cortex tissues and HK-2 cells, and reverse-transcribed into cDNA using a commercial reverse transcription kit. qRT-PCR amplification was performed with SYBR Green qPCR master mix on a real-time PCR instrument. Primers for the corresponding human and rat target genes were designed using NCBI Primer-BLAST, and their specificity was verified by BLAST analysis. All primer sequences are provided in Supplementary Table S2. The amplification procedure included pre-denaturation and 40 cycles of denaturation, annealing, and extension. All samples were tested in triplicate. Relative mRNA expression levels were calculated using the $2^{-}\Delta\Delta Ct$ method.

2.14 Cell Viability Assay (CCK-8)

HK-2 cells in the logarithmic growth phase were seeded in 96-well plates with 100 μL complete medium per well. After 24-hour incubation at 37 ℃ with 5% CO_2 to allow full cell adherence, cells were treated with different concentrations of LPS for 12 h. Subsequently, 10 μL CCK-8 reagent was added to each well, followed by gentle shaking and 2-hour dark incubation at 37 ℃ with 5% CO_2. The absorbance value at 450 nm was measured using a microplate reader to evaluate cell viability.

2.14 ATP Content Detection

ATP levels in rat renal cortex tissues and HK-2 cells were detected strictly in accordance with the instructions of a commercial ATP detection kit. Samples were fully lysed with kit-matched lysis buffer on ice and centrifuged at 12000×g for 5 min at 4 ℃ to collect supernatants. A standard curve was generated via gradient dilution of ATP standard solution. Supernatant samples and luciferase working solution were added to opaque 96-well plates. After room-temperature incubation, luminescence values were measured using a multifunctional microplate reader. ATP concentrations were calculated based on the standard curve and normalized to total protein content to obtain relative ATP levels.

2.15 FAO Rate Detection

FAO rates in rat renal cortex tissues and HK-2 cells were determined using a commercial fatty acid oxidation rate detection kit. Samples were lysed and centrifuged on ice to collect supernatants. The reaction system was prepared and incubated at 37 ℃ according to kit protocols, and absorbance at 485 nm was detected with a multifunctional microplate reader. FAO rates were calculated via standard curve fitting and normalized to total protein content to obtain relative FAO activity in each group.

2.16 Dual-Luciferase Reporter Assay

A dual-luciferase reporter assay was performed to verify the transcriptional regulatory effect of KLF5 on PGC-1α. HK-2 cells were co-transfected with a pGL3-basic luciferase reporter plasmid carrying the *PPARGC1A* promoter, a pRL-TK internal reference plasmid, or empty control plasmid. All plasmids were synthesized by Saiwen Innovation Biotechnology. After 30–48 hours of culture, cells were lysed for luciferase activity detection. Firefly luciferase activity was normalized to Renilla luciferase activity to correct transfection efficiency, and relative luciferase activity reflected the transcriptional activity of the *PPARGC1A*promoter.

2.17 Clinical Study Subjects

This study was designed as a retrospective observational study, enrolling adult inpatients from the First Affiliated Hospital of Harbin Medical University, including 18 SA-AKI patients and 14 control subjects. SA-AKI was diagnosed based on concurrent sepsis and acute kidney injury meeting KDIGO criteria, with AKI defined as a ≥ 0.3 mg/dL increase in serum creatinine within 48 hours. Detailed inclusion and exclusion criteria are provided in Supplementary Table S2. Circulating KLF5 concentrations were measured via enzyme-linked immunosorbent assay (ELISA). Renal biochemical indices were detected using an automatic biochemical analyzer. For statistical analysis, the Wilcoxon rank-sum test was used to compare serum KLF5 levels between the SA-AKI and control groups. Spearman correlation analysis was applied to assess the correlation between serum KLF5 levels, serum creatinine, and eGFR. Receiver operating characteristic (ROC) curve analysis was performed to evaluate the diagnostic efficacy of serum KLF5 for SA-AKI.

2.18 Statistical Analysis

All experimental data are presented as mean ± standard error of the mean (SEM). All experiments were independently repeated no less than three times. Statistical analysis was conducted using GraphPad

Prism 10 software. Independent samples t-test was used for two-group comparisons, while one-way analysis of variance (ANOVA) followed by Tukey's post-hoc test was applied for multiple-group comparisons. $P < 0.05$ was considered statistically significant.

3. Results

3. 1 Serum KLF5 Level is Significantly Upregulated in SA-AKI Patients

We found that serum KLF5 levels were significantly elevated in patients with sepsis-associated acute kidney injury (SA-AKI). Serum KLF5 concentrations were significantly higher in the SA-AKI group than in the control group (Wilcoxon rank-sum test, Fig. 1a). Receiver operating characteristic (ROC) curve analysis gave an AUC of 0.937 for distinguishing SA-AKI from controls, indicating excellent diagnostic performance of serum KLF5 (Fig. 1b). These findings suggest that elevated KLF5 is closely associated with the onset and progression of SA-AKI.

Figure 1 KLF5 expression is upregulated in clinical SA-AKI samples and LPS-induced rat SA-AKI models (**a**) Serum KLF5 levels in SA-AKI patients and control subjects, analyzed by Wilcoxon rank-sum test. (**b**) ROC curve for evaluating the diagnostic value of serum KLF5 for SA-AKI. (**c**) Transcriptomic expression levels of *Klf5* in renal tissues at the three time points. (**d-f**) Volcano plots showing differentially expressed genes (DEGs) in renal tissues at 3 h, 6 h and 12 h after LPS treatment. (**g**) Venn diagram showing overlapping DEGs across the three time points. (**h**) GO functional enrichment analysis of the overlapping DEGs. (**i**) KEGG pathway enrichment analysis of the overlapping DEGs. (**j-k**) Serum levels of creatinine (Scr) and blood urea nitrogen (BUN) in control and LPS-treated rats. (**l**) Representative images of H&E staining of renal tissues. n = 4 rats per group. Scale bar = 100 μm. *P < 0.05, **P < 0.01, ****P < 0.0001.

3.2 KLF5 displays sustained overexpression in renal tissues of SA-AKI rats.

To further explore the biological function of KLF5 in SA-AKI, an SA-AKI rat model was established via intraperitoneal injection of 10 mg/kg LPS. Rats were euthanized at 3, 6, and 12 h post-treatment, and renal tissues were collected for transcriptome sequencing. DEGs were screened using RStudio with thresholds of $P < 0.05$ and $|\log2 \text{ fold change}| > 1$. The results revealed persistent and significant KLF5 upregulation at all three time points (Fig. 1c–f), with log2FC values of 4.63, 4.09, and 3.84 at 3, 6, and 12 h, respectively. Key FAO-related DEGs, including Plin2, Ppara, and Ppargc1a, were highlighted in volcano plots. A total of 1385 overlapping DEGs were identified across the three time points (Fig. 1g). GO functional enrichment analysis indicated that these DEGs were primarily enriched in LPS response and inflammatory response pathways (Fig. 1h). KEGG pathway analysis showed significant enrichment in lipid metabolism and atherosclerosis pathways, which are closely related to FAO (Fig. 1i). Accordingly, KLF5 and FAO dysfunction were selected as the core molecular and phenotypic indicators for subsequent mechanistic exploration.

3.3 KLF5 is Upregulated in LPS-Induced SA-AKI Rat Tissues and HK-2 Cells

Our preliminary experiments showed that renal injury was most severe 12 h after LPS stimulation; therefore, this time point was selected for subsequent in vivo investigation. Renal function analysis showed that Scr and BUN levels were significantly increased in the LPS 12 h group, with Scr levels more than 1.5-fold higher than those in the control group, confirming successful establishment of the SA-AKI model (Fig. 1j-k). H&E staining showed that LPS treatment induced marked glomerular congestion, extensive tubular dilation, tubular epithelial swelling and vacuolar degeneration, partial epithelial necrosis and sloughing, interstitial edema, and inflammatory cell infiltration, leading to exacerbated renal pathological injury (Fig. 1l). Western blot analysis confirmed significantly elevated expression of renal injury and inflammatory markers (KIM-1, NGAL, IL-6, IL-1β, TNF-α) in LPS-treated rats, indicating severe renal dysfunction and inflammatory response (Fig. 2a). Immunohistochemical staining revealed an increased KLF5-positive area in LPS-injured renal tissues (Fig. 2b). Consistent with histological results, qRT-PCR and Western blotting confirmed significant upregulation of KLF5 mRNA and protein expression in LPS-treated renal tissues (Fig. 2c). In vitro cellular assays yielded consistent results. To determine the optimal LPS concentration, HK-2 cells were treated with various concentrations of LPS for 12 h. Cell viability was significantly decreased at an LPS concentration of 40 μg/mL (Supplementary Fig. S1a); therefore, 40 μg/mL LPS was used for all subsequent cellular experiments. LPS stimulation induced inflammatory injury and markedly increased KLF5 mRNA and protein levels in HK-2 cells (Fig. 2d–e). Collectively, these findings confirm that KLF5 expression is significantly elevated both in vivo and in vitro during SA-AKI progression.

Figure 2 KLF5 expression is elevated in SA-AKI both in vivo and in vitro (**a**) Representative Western blot analysis of KLF5, renal injury and inflammatory markers (KIM-1, NGAL, IL-6, IL-1β, TNF-α) in rat renal tissues. (**b**) Representative images of immunohistochemical staining of KLF5 in rat renal tissues. n = 4 rats per group. Scale bar = 100 μm. (**c**) mRNA levels of KLF5 in rat renal tissues detected by qRT-PCR. (**d**) mRNA levels of KLF5 in HK-2 cells detected by qRT-PCR. (**e**) Representative Western blot analysis of KLF5, renal injury and inflammatory markers (KIM-1, NGAL, IL-6, IL-1β, TNF-α) in HK-2 cells with or without LPS treatment. Data are the mean ± SEM of at least three independent experiments. *P < 0.05, **P < 0.01, ***P < 0.001, ****P < 0.0001

3.4 FAO Function is Severely Impaired in SA-AKI Renal Tissues and HK-2 Cells

Oil Red O staining and transmission electron microscopy (TEM) revealed massive lipid droplet accumulation in LPS-injured rat renal tissues (Fig. 3a–b), accompanied by significantly increased renal TG and NEFA contents, indicating marked renal lipid deposition in SA-AKI models (Fig. 3c–d). Analysis of energy metabolism showed reduced FAO rates (Fig. 3e) and suppressed ATP production (Fig. 3f) in SA-AKI renal tissues, reflecting severe FAO dysfunction. Immunofluorescence staining showed that the positively stained areas of CPT1A and PPARα in rat kidney tissues decreased at 12 h after LPS treatment

(Fig. 3h). qRT-PCR and Western blotting further confirmed decreased mRNA and protein expression of the key FAO regulators PPARα and CPT1A in LPS-treated renal tissues (Fig. 3g–j). In vitro, LPS stimulation also triggered abnormal lipid accumulation, blocked ATP synthesis, reduced FAO activity, and downregulated the expression of FAO-related genes in HK-2 cells (Supplementary Fig. S1b). Collectively, these results demonstrate that FAO homeostasis is severely disrupted in SA-AKI.

Figure 3 Fatty acid oxidation function is impaired in SA-AKI renal tissues and HK-2 cells (**a**) Representative images of Oil Red O staining of lipid droplets in rat renal tissues. (**b**) Representative TEM images showing mitochondrial and lipid droplet ultrastructure in renal tubular epithelial cells. n = 4 rats per group. (**c**) Levels of triglyceride (TG) in rat renal tissues. (**d**) Levels of non-esterified fatty acid (NEFA) in rat renal tissues. (**e**) FAO rate in rat renal tissues. (**f**) ATP content in rat renal tissues. (**g**) mRNA levels of *PPARA* in rat renal tissues. (**h**) Representative images of immunofluorescence staining of CPT1A and PPARα in rat renal tissues. n = 4 rats per group. Scale bar = 100 μm. (**i**) mRNA levels of *CPT1A* in rat renal tissues. (**j**) Protein levels of PPARα and CPT1A in rat renal tissues detected by Western blot. Data are the mean ± SEM of at least three independent experiments. *P < 0.05, **P < 0.01, ***P < 0.001, ****P < 0.0001

3.5 Pharmacological KLF5 Inhibition Ameliorates Renal FAO Impairment in SA-AKI Rats

To clarify the regulatory effect of KLF5 on renal FAO function, in vivo pharmacological intervention was performed using ML264, a selective KLF5 inhibitor. ML264 was dissolved in normal saline and administered at a dose of 10 mg/kg to inhibit endogenous KLF5 activity. The results showed that ML264 alleviated renal injury (Fig. 4a–c) and lipid accumulation (Fig. 4d–f) in rats after LPS stimulation. Meanwhile, KLF5 inhibition significantly restored the suppressed renal ATP content and FAO rate (Fig. 4g–h). Immunohistochemical staining showed that the positively stained areas of CPT1A and PPARα in rat renal tissues were reduced at 12 h after LPS stimulation (Fig. 4i). Western blotting confirmed that ML264 treatment effectively suppressed renal KLF5 expression and restored the protein levels of PPARα and CPT1A, the core downstream effectors of FAO signaling (Fig. 4j). These in vivo results indicate that KLF5 inhibition attenuates renal lipid deposition and FAO dysfunction, thereby mitigating LPS-induced renal injury

Figure 4 Pharmacological inhibition of KLF5 by ML264 ameliorates renal FAO impairment in SA-AKI rats(**a-c**) Evaluation of renal injury after ML264 treatment: representative H&E staining, serum Scr and BUN levels. (**d-f**) Detection of lipid accumulation after ML264 treatment: representative Oil Red O staining, renal TG and NEFA levels. n = 4 rats per group. Scale bar = 100 μm. (**g-h**) Renal ATP content and FAO rate after ML264 treatment. (**i**). Representative images of immunohistochemical staining of CPT1A and PPARα in rat renal tissues after ML264 treatment. n = 4 rats per group. Scale bar = 100 μm. (**j**) Representative Western blot and quantitation of KLF5, PPARα and CPT1A protein levels in renal tissues. Data are the mean ± SEM of at least three independent experiments. *P < 0.05, **P < 0.01, ***P < 0.001, ****P < 0.0001

3.6 KLF5 Knockdown Alleviates LPS-Triggered FAO Impairment in HK-2 Cells

In vitro siRNA-mediated knockdown experiments were performed to verify the in vivo findings. qRT-PCR analysis showed that all three designed siRNA sequences efficiently silenced KLF5 expression, with a knockdown efficiency of 70%–80% (Fig. 5a), and siKLF5-1, which showed the highest knockdown efficiency, was selected for subsequent functional experiments. Western blotting results confirmed that transfection with siKLF5-1 significantly downregulated KLF5 protein expression in HK-2 cells (Fig. 5b). The suppressed expression of PPARα and CPT1A in LPS-stimulated HK-2 cells was significantly restored after KLF5 silencing (Fig. 5c). Moreover, functional experiments showed that KLF5 knockdown effectively reversed LPS-induced intracellular lipid accumulation and energy metabolism disorders (Fig. 5d-f). These in vitro results further confirmed that KLF5 knockdown rescued LPS-mediated FAO dysfunction in renal tubular cells.

3.7 KLF5 Transcriptionally Downregulates PGC-1α Expression During SA-AKI

To elucidate the molecular mechanism underlying KLF5-mediated FAO regulation, we first analyzed lipid metabolism-related DEGs from transcriptomic data using the STRING database, which predicted a potential interaction between KLF5 and PGC-1α (Fig. 6a). Subsequent target gene prediction using the GTRD (Gene Transcription Regulation Database) identified *PPARGC1A* (the gene encoding PGC-1α) as a high-confidence candidate target of KLF5, with multiple specific KLF5 binding peaks enriched in its regulatory region (Fig. 6b). Sequence alignment further verified potential KLF5 binding sites in the promoter region (± 5 kb upstream of the transcription start site) of *PPARGC1A*. JASPAR database analysis confirmed that this region contains the classical conserved KLF5 binding motif (Fig. 6c). A dual-luciferase reporter system carrying the *PPARGC1A* promoter was constructed and co-transfected with a KLF5 overexpression plasmid or an empty vector into HK-2 cells (Fig. 6d). The results showed that KLF5 overexpression significantly inhibited the luciferase activity of the *PPARGC1A* promoter, verifying that KLF5 directly binds to the conserved sequence of the *PPARGC1A* promoter and exerts negative transcriptional regulation.

3.8 PGC-1α Knockdown Abolishes the Protective Effects of KLF5 Inhibition on FAO Function

Rescue experiments were performed to further confirm that KLF5 regulates FAO function in a PGC-1α-dependent manner. In vivo, LPS stimulation significantly downregulated renal PGC-1α expression in wild-type rats, whereas pharmacological KLF5 inhibition effectively restored PGC-1α protein levels (Fig. 6e–f). Consistently, in vitro KLF5 knockdown also reversed LPS-induced PGC-1α downregulation in HK-2 cells (Fig. 6g–h). To verify the core role of PGC-1α in this regulatory axis, we transfected three siRNA sequences targeting PGC-1α into HK-2 cells and selected the most efficient one for subsequent rescue

assays (Fig. 7a–b). HK-2 cells were pre-transfected with KLF5 siRNA alone or co-transfected with PGC-1α siRNA before LPS stimulation. Functional results showed that KLF5 knockdown alone significantly rescued LPS-induced FAO suppression, whereas concurrent PGC-1α knockdown completely abolished the metabolic protective effects of KLF5 silencing (Fig. 7d–f). Western blotting further confirmed that PGC-1α knockdown abrogated the KLF5 inhibition-mediated recovery of PPARα and CPT1A expression (Fig. 7c). These rescue findings demonstrate that PGC-1α is an indispensable downstream mediator of KLF5-regulated FAO dysfunction in SA-AKI.

4. Discussion

The pathogenesis of sepsis-associated acute kidney injury (SA-AKI) involves complex pathological processes, including systemic inflammation, mitochondrial structural and functional abnormalities, and renal tubular metabolic disorders [26]. Current clinical management of SA-AKI is largely limited to supportive care, such as anti-infective therapy, fluid resuscitation, and renal replacement therapy, with no targeted strategies to reverse tubular metabolic dysfunction [27]. In recent years, restoring impaired tubular metabolism to halt SA-AKI progression and improve patient outcomes has become a major focus in nephrology [11, 23, 28, 29]. Against this background, the present study focuses on the transcriptional regulatory mechanism of KLF5 in lipid metabolism, aiming to identify key targets in tubular energy metabolic disorders, clarify the underlying pathogenesis of SA-AKI, and provide new insights for targeted clinical intervention.

We detected significantly elevated serum KLF5 levels in an independent cohort of SA-AKI patients, with good diagnostic performance (AUC = 0.937). Consistent with this finding, a clinical study of 120 patients with sepsis reported elevated serum KLF5 in SA-AKI cases [30]. However, that study remained at the correlational level and did not address the underlying mechanism, leaving it unclear whether the rise in serum KLF5 represents a cause or a consequence of renal injury. Building on the clinical observation of elevated KLF5, we further found in both in vivo and in vitro experiments that LPS stimulation upregulated KLF5 in tubular epithelial cells, and this increase was associated with fatty acid oxidation dysfunction and the severity of injury. These data suggest that KLF5 elevation may not be merely a secondary change after injury but rather actively participates in the impairment of tubular fatty acid oxidation and the aggravation of renal damage, thereby linking the clinical relevance of KLF5 to a specific pathogenic mechanism.

We performed transcriptomic analysis of renal tissues from LPS-treated rats at 3, 6, and 12 h, and found that Klf5 was significantly upregulated as early as 3 h (log2FC = 4.63) and remained elevated until 12 h. Western blotting further confirmed that KLF5 protein levels increased after LPS treatment, accompanied by corresponding increases in inflammatory and injury markers such as KIM-1, NGAL, and IL-6. This finding is consistent with a previous study in LPS-induced AKI, which also observed KLF5 upregulation accompanied by elevated inflammatory markers and showed that KLF5 aggravates inflammation through the NF-κB pathway, with KLF5 silencing reducing KIM-1 and NGAL expression [19]. However, in that study KLF5 was detected at 24 h, a time point at which injury is already established. In AKI-to-CKD

transition models, KLF5 was examined at day 3 or day 14, with a focus on its cooperation with c-JUN to promote SNAI1 transcription and fibrosis [31], or on ferroptosis via the HDAC3/Gpx4 axis [32]. These time points are much later than our 3–12 h observation window. By contrast, our data captured sustained KLF5 elevation within the early 3–12 h window. Moreover, we selected the 12 h time point for subsequent in-depth investigation based on our group's previous finding that renal injury was most severe at this time point but still relatively early in the disease process. This approach allowed us to examine both fully established renal injury and the early upstream actions of KLF5, representing a clear advantage over previous reports.

Further analysis of the transcriptomic data from LPS-treated rat kidneys revealed significant enrichment of lipid metabolism-related pathways, widespread downregulation of FAO-related genes, and a negative correlation with Klf5 expression. This observation directly linked KLF5 to tubular fatty acid oxidation. Subsequent functional assessments in the same LPS model showed decreased FAO rates, reduced ATP production, massive lipid droplet accumulation on Oil Red O staining and electron microscopy, elevated TG and NEFA levels, and decreased PPARα and CPT1A expression. These changes are consistent with the FAO impairment reported previously, but prior studies have mainly focused on positive regulators or pharmacological interventions. For example, FXR improves FAO through PPARγ in cisplatin-induced AKI [33]; fenofibrate restores FAO by activating AMPK in LPS-induced SA-AKI [9]; SP1 influences FAO through SIRT1/ACLY in ischemia-reperfusion injury [34]; and KLF15 positively regulates FAO by interacting with PPARα [35]. In contrast to this positive regulation, our results identify KLF5 as an endogenous negative regulator of FAO that directly causes FAO impairment by inhibiting PGC-1α transcription and thereby downregulating PPARα/CPT1A. This finding identifies an endogenous negative regulatory mechanism for FAO in kidney injury and explains how FAO can be actively suppressed without exogenous intervention. Because Klf5 is upregulated early and remains persistently elevated, it may drive disturbances in tubular energy metabolism from the initial stage of injury, suggesting that early blockade of KLF5 could interrupt the initiation of FAO suppression at an upstream level.

To define the mechanism by which KLF5 regulates fatty acid oxidation, we screened lipid metabolism-related genes from the transcriptomic differentially expressed genes and performed interaction analysis using the STRING database. The results suggested a potential interaction between KLF5 and PGC-1α, leading us to select PGC-1α as a candidate downstream target. Subsequent analyses using the GTRD and JASPAR databases identified KLF5 binding sites and conserved motifs in the *PPARGC1A* promoter region. Dual-luciferase reporter assays further confirmed that KLF5 overexpression significantly inhibited the promoter activity, indicating that KLF5 directly binds to the *PPARGC1A* promoter and represses its transcription. Previous studies on PGC-1α downregulation in AKI have mainly addressed post-translational modifications and protein interactions, such as SIRT1-mediated deacetylation [36], ALDH2-mediated promotion of nuclear translocation [37], TEAD1 binding [38], or indirect transcriptional inhibition through CD44/MAPK/NF-κB [39]. These mechanisms act on the existing PGC-1α protein or depend on upstream signal transduction. KLF5-mediated negative regulation of fatty acid oxidation has also been reported in metabolic dysfunction-associated fatty liver disease, in which KLF5 promotes ubiquitination and degradation of CPT1α through RNF90, a post-translational mechanism [40]. In the

kidney, however, KLF5 directly binds to the *PPARGC1A* promoter and represses its transcription. This regulatory mode acts at a more upstream level, affecting the expression of the entire FAO-related gene network rather than the activity or stability of a single protein, and thus provides a new upstream mechanistic explanation for PGC-1α downregulation in sepsis-induced kidney injury.

To validate the pathogenic role of the KLF5–PGC-1α–FAO axis, we first used ML264 to inhibit KLF5 in vivo. We found that ML264 not only improved renal function and tubular injury in SA-AKI rats but also restored renal FAO rates and ATP content and reduced lipid deposition. Previous studies on ML264 have primarily reported its anti-inflammatory and anti-pyroptotic effects [18], and its attenuation of ferroptosis [32], its ability to improve cell cycle arrest and fibrosis [41], but metabolic recovery has not been examined. Therefore, the metabolic protection observed here represents a previously unrecognized effect of ML264. To further verify the direct regulatory effect of KLF5 on FAO, we knocked down KLF5 using siRNA in vitro. KLF5 knockdown reversed LPS-induced PGC-1α downregulation, FAO impairment, and lipid accumulation, whereas co-knockdown of PGC-1α completely abolished the protective effects of KLF5 inhibition. This dual-intervention design demonstrates that KLF5 regulation of FAO is dependent on PGC-1α and identifies PGC-1α as an indispensable downstream mediator of this signaling axis. Compared with previous studies that examined KLF5 or FAO in isolation, our results establish KLF5, PGC-1α, and FAO as components of a single pathogenic pathway by establishing a causal link, providing a more complete target basis for metabolic intervention in SA-AKI.

This study has several limitations. First, we used only the LPS-induced endotoxemia model, rather than the more clinically relevant cecal ligation and puncture (CLP) sepsis model, which limits the generalizability of our conclusions. Second, the core signaling axis was validated only in rat renal tissues and human tubular cell lines, without confirmation in SA-AKI patient specimens, thus limiting clinical translation. Third, tubular-specific Klf5 knockout animal models were not established; therefore, systemic administration of ML264 and transient siRNA-mediated knockdown cannot rule out contributions from KLF5 in other cell types or potential off-target effects.

In conclusion, this study demonstrates that aberrant KLF5 upregulation during SA-AKI progression transcriptionally represses PGC-1α, thereby suppressing PPARα/CPT1A-mediated FAO signaling and inducing renal tubular lipid accumulation and disturbed energy metabolism, ultimately exacerbating renal pathological injury. Our findings reveal a previously unappreciated metabolic function of KLF5 in renal lipid homeostasis and clarify the upstream transcriptional repression of PGC-1α under septic conditions, providing experimental evidence for targeted metabolic intervention in SA-AKI.

Declarations

Competing interests

All the authors declared no competing interests.

Supporting information

This article contains supporting information.

Funding

No funding was received for this study.

Author Contribution

J.L., Y.D., and P.L. designed and performed experiments, analyzed data, and revised the manuscript. Y.Z. and W.H. analyzed data, prepared and maintained ethics board protocols, and inputted and analyzed data. M.X. performed experiments and analyzed data. W.L. reviewed the manuscript. Y.J. obtained funding, designed experiments, analyzed data, and wrote and revised the manuscript. All authors reviewed the manuscript.

Acknowledgments

The authors have no acknowledgements to declare.

Data Availability

The transcriptomic data have been deposited in NCBI's Gene Expression Omnibus and are accessible through GEO Series accession number GSE337961 (https://www.ncbi.nlm.nih.gov/geo/query/acc.cgi?acc=GSE337961).

References

1. Takeuchi, T., A. H. Flannery, and L. J. Liu et al. 2025. Epidemiology of sepsis–associated acute kidney injury in the ICU with contemporary consensus definitions. *Critical Care* 29:128. https://doi.org/10.1186/s13054-025-05351-5
2. Poston, J. T., and J. L. Koyner. 2019. Sepsis associated acute kidney injury. *Bmj*. https://doi.org/10.1136/bmj.k4891
3. Zarbock, A., M. K. Nadim, and P. Pickkers et al. 2023. Sepsis–associated acute kidney injury: consensus report of the 28th Acute Disease Quality Initiative workgroup. *Nature Reviews Nephrology* 19:401–417. https://doi.org/10.1038/s41581-023-00683-3
4. Mehta, R. L., E. A. Burdmann, and J. Cerdá et al. 2016. Recognition and management of acute kidney injury in the International Society of Nephrology 0by25 Global Snapshot: a multinational cross–

sectional study. *The Lancet* 387:2017–2025. https://doi.org/10.1016/S0140-6736(16)30240-9

5. Ostermann, M., N. Lumlertgul, and R. Jeong et al. 2025. Acute kidney injury. *The Lancet* 405:241–256. https://doi.org/10.1016/S0140-6736(24)02385-7
6. Kang, H. M., S. H. Ahn, and P. Choi et al. 2015. Defective fatty acid oxidation in renal tubular epithelial cells has a key role in kidney fibrosis development. *Nature Medicine* 21:37–46. https://doi.org/10.1038/nm.3762
7. Carney, E. F. 2016. Metabolism: Energy–efficient transport in the kidney. *Nature Reviews Nephrology* 12:443. https://doi.org/10.1038/nrneph.2016.83
8. Chung, K. W., E. K. Lee, and M. K. Lee et al. 2018. Impairment of PPARα and the Fatty Acid Oxidation Pathway Aggravates Renal Fibrosis during Aging. *Journal of the American Society of Nephrology* 29:1223–1237. https://doi.org/10.1681/ASN.2017070802
9. Zeng, S., J. Wang, and C. Guan et al. 2025. Fenofibrate alleviates sepsis–associated acute kidney injury by enhancing renal fatty acid oxidation. *BMC Pharmacology & Toxicology* 26:160. https://doi.org/10.1186/s40360-025-00997-x
10. Iwaki, T., B. G. Bennion, and E. K. Stenson et al. 2019. PPARα contributes to protection against metabolic and inflammatory derangements associated with acute kidney injury in experimental sepsis. *Physiological Reports* 7:e14078. https://doi.org/10.14814/phy2.14078
11. Pollak, N. M., M. Hoffman, and I. J. Goldberg et al. 2018. Krüppel–like factors: Crippling and un–crippling metabolic pathways. *JACC: Basic to Translational Science* 3:132–156. https://doi.org/10.1016/j.jacbts.2017.09.001
12. Li, J., L. Liu, and W. Q. Zhou et al. 2021. Roles of Krüppel–like factor 5 in kidney disease. *Journal of Cellular and Molecular Medicine* 25:2342–2355. https://doi.org/10.1111/jcmm.16332
13. Huang, H., J. Chen, and P. Zhong et al. 2026. KLF5–driven TAZ–FASN signaling reprograms fatty acid metabolism to support Treg differentiation in lung cancer. *Journal of Translational Medicine*. https://doi.org/10.1186/s12967-026-08557-5
14. Fujiu, K., I. Manabe, and R. Nagai. 2011. Renal collecting duct epithelial cells regulate inflammation in tubulointerstitial damage in mice. *The Journal of Clinical Investigation* 121:3425–3441. https://doi.org/10.1172/JCI57582
15. Chen, W. C., H. H. Lin, and M. J. Tang. 2015. Matrix–Stiffness–Regulated Inverse Expression of Krüppel–Like Factor 5 and Krüppel–Like Factor 4 in the Pathogenesis of Renal Fibrosis. *The American Journal of Pathology* 185:2468–2481. https://doi.org/10.1016/j.ajpath.2015.05.019
16. Zhang, X., J. Chen, and R. Lin et al. 2024. Lactate drives epithelial–mesenchymal transition in diabetic kidney disease via the H3K14la/KLF5 pathway. *Redox Biology* 75:103246. https://doi.org/10.1016/j.redox.2024.103246
17. Cippà, P. E., B. Sun, and J. Liu et al. 2018. Transcriptional trajectories of human kidney injury progression. *JCI Insight* 3:e123151. https://doi.org/10.1172/jci.insight.123151
18. Lu, J., Y. Hou, and S. X. Liu et al. 2024. Acetyl–CoA synthetase 2 induces pyroptosis and inflammation of renal epithelial tubular cells in sepsis–induced acute kidney injury by upregulating

the KLF5/NF–κB pathway. *Cell Communication and Signaling* 22:187. https://doi.org/10.1186/s12964-024-01556-3

19. Ban, K. Y., G. Y. Nam, and D. Kim et al. 2022. Prevention of LPS–Induced Acute Kidney Injury in Mice by Bavachin and Its Potential Mechanisms. *Antioxidants* 11: 2096. https://doi.org/10.3390/antiox11112096
20. Yu, H. C., L. Bai, and L. Jin et al. 2025. SLC25A35 enhances fatty acid oxidation and mitochondrial biogenesis to promote the carcinogenesis and progression of hepatocellular carcinoma by upregulating PGC–1α. *Cell Communication and Signaling* 23:130. https://doi.org/10.1186/s12964-025-02109-y
21. Song, J., J. Ye, and N. Sheng et al. 2026. Ramulus Mori (Sangzhi) Alkaloids (SZ–A) exert a renoprotective effect by activating PGC–1α to mediate fatty acid oxidation and mitochondrial homeostasis. *Phytomedicine* 150:157743. https://doi.org/10.1016/j.phymed.2025.157743
22. Wang, X., Z. Li, and C. Liu et al. 2025. Multi–target renal protection in AKI: Exercise–mediated coordination of AMPK energy homeostasis, mTOR autophagy regulation, and NF–κB inflammatory control. *Free Radical Biology and Medicine* 240:397–409. https://doi.org/10.1016/j.freeradbiomed.2025.08.030
23. Zhou, Y., X. Zeng, and Y. Zheng et al. 2026. Asperosaponin VI ameliorates acute kidney injury via restoring metabolic–oxidative homeostasis in NRF2 and PPARα dependent manners. *Phytomedicine* 153:157957. https://doi.org/10.1016/j.phymed.2026.157957
24. Deng, Y., C. Xu, and J. Ma et al. 2026. Schisandrin B Attenuates Renal Fibrotic Remodeling in Association with Restoration of a PPARα–Related Tubular Fatty–Acid Oxidation Program. *Biomedicines* 14:1351. https://doi.org/10.3390/biomedicines14061351
25. Wang, L., Y. Xie, and B. Xiao et al. 2024. Isorhamnetin alleviates cisplatin–induced acute kidney injury via enhancing fatty acid oxidation. *Free Radical Biology and Medicine* 212:22–33. https://doi.org/10.1016/j.freeradbiomed.2023.12.010
26. Liu, L., X. Ning, and L. Wei et al. 2022. Twist1 downregulation of PGC–1α decreases fatty acid oxidation in tubular epithelial cells, leading to kidney fibrosis. *Theranostics* 12:3758–3775. https://doi.org/10.7150/thno.71722
27. Levin, A. 2018. Global challenges in kidney diseases. *Nephrology Dialysis Transplantation* 33:371–372. https://doi.org/10.1093/ndt/gfy037
28. Livingston, M. J., S. Shu, and Y. Fan et al. 2023. Tubular cells produce FGF2 via autophagy after acute kidney injury leading to fibroblast activation and renal fibrosis. *Autophagy* 19:256–277. https://doi.org/10.1080/15548627.2022.2072054
29. Gao, Z., and X. Chen. 2022. Fatty Acid β–Oxidation in Kidney Diseases: Perspectives on Pathophysiological Mechanisms and Therapeutic Opportunities. *Frontiers in Pharmacology* 13:805281. https://doi.org/10.3389/fphar.2022.805281
30. Hu, J., Y. Lin, and Y. Wang et al. 2024. Diagnostic and Prognostic Values of KLF5 and RUNX1 in Acute Kidney Injury in Septic Patients. *Applied Biochemistry and Biotechnology* 196:8306–8316.

https://doi.org/10.1007/s12010-024-04956-w

31. Gu, S., H. Feng, and X. Li et al. 2025. Targeting WNT5A noncanonical signaling attenuates renal fibrosis progression in acute kidney injury. *Molecular Therapy* 33:5248–5262. https://doi.org/10.1016/j.ymthe.2025.06.039
32. Zhang, L., F. Chen, and J. Dong et al. 2023. HDAC3 aberration–incurred GPX4 suppression drives renal ferroptosis and AKI–CKD progression. *Phytomedicine* 142. https://doi.org/10.1016/j.phymed.2025.156765
33. Xu, S., P. Jia, and Y. Fang et al. 2022. Nuclear farnesoid X receptor attenuates acute kidney injury through fatty acid oxidation. *Kidney International* 101:987–1002. https://doi.org/10.1016/j.kint.2022.01.029
34. Wu, H., L. Wang, and P. Kang et al. 2024. The SP1/SIRT1/ACLY signaling axis mediates fatty acid oxidation in renal ischemia–reperfusion–induced renal fibrosis. *International Immunopharmacology* 132:112002. https://doi.org/10.1016/j.intimp.2024.112002
35. Piret, S. E., A. A. Attallah, and X. Gu et al. 2021. Loss of proximal tubular transcription factor Krüppel–like factor 15 exacerbates kidney injury through loss of fatty acid oxidation. *Kidney International* 100:1250–1267. https://doi.org/10.1016/j.kint.2021.08.031
36. Huang, Y., E. Zhao, and G. Zhao et al. 2026. H3K18 lactylation–mediated SPHK1–SIRT1 feedback loop accelerates pyroptosis of tubular epithelial cells in sepsis–associated acute kidney injury. *Theranostics* 16:4768–4786. https://doi.org/10.7150/thno.122991
37. Li, J., X. Shi, and Z. Chen et al. 2023. Aldehyde dehydrogenase 2 alleviates mitochondrial dysfunction by promoting PGC–1α–mediated biogenesis in acute kidney injury. *Cell Death & Disease* 14:45. https://doi.org/10.1038/s41419-023-05557-x
38. Tran, M., B. Jiao, and H. Du et al. 2025. TEAD1 Prevents Necroptosis and Inflammation in Cisplatin–Induced Acute Kidney Injury Through Maintaining Mitochondrial Function. *International Journal of Biological Sciences* 21:565–578. https://doi.org/10.7150/ijbs.104335
39. Huang, J., P. Meng, and Y. Liang et al. 2025. Tubular CD44 plays a key role in aggravating AKI through NF–κB p65–mediated mitochondrial dysfunction. *Cell Death & Disease* 16:119. https://doi.org/10.1038/s41419-025-07438-x
40. Yan, F. J., N. Zhang, and S. H. Li et al. 2026. RNF90 promotes hepatic steatosis by degrading CPT1α to suppress fatty acid oxidation. *Journal of Biological Chemistry* 302:111231. https://doi.org/10.1016/j.jbc.2026.111231

Figures

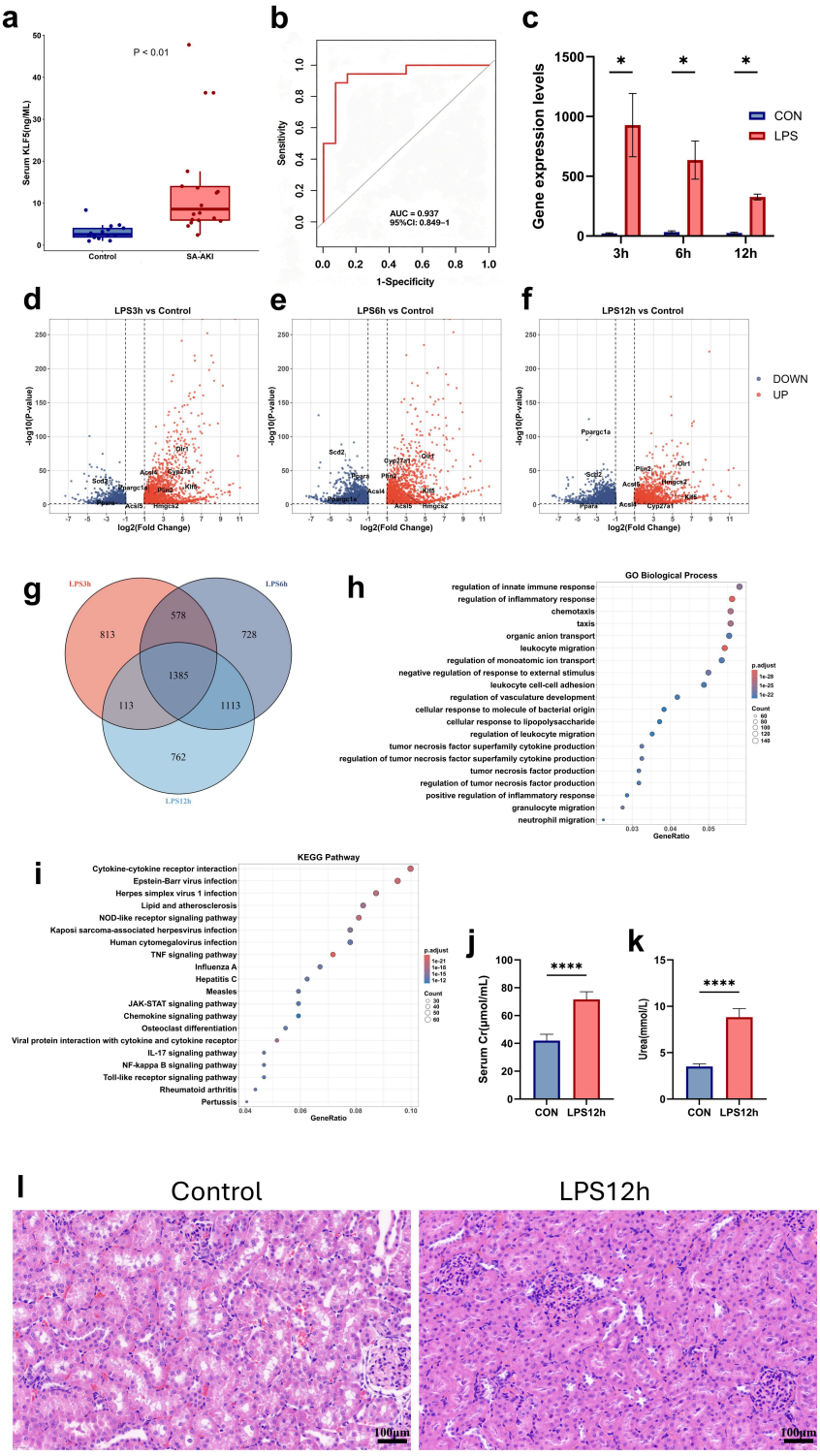


Figure 1

KLF5 expression is upregulated in clinical SA-AKI samples and LPS-induced rat SA-AKI models (**a**) Serum KLF5 levels in SA-AKI patients and control subjects, analyzed by Wilcoxon rank-sum test. (**b**) ROC curve for evaluating the diagnostic value of serum KLF5 for SA-AKI. (**c**) Transcriptomic expression levels of *Klf5* in renal tissues at the three time points. (**d-f**) Volcano plots showing differentially expressed genes (DEGs) in renal tissues at 3 h, 6 h and 12 h after LPS treatment. (**g**) Venn diagram showing overlapping

DEGs across the three time points. (**h**) GO functional enrichment analysis of the overlapping DEGs. (**i**) KEGG pathway enrichment analysis of the overlapping DEGs. (**j-k**) Serum levels of creatinine (Scr) and blood urea nitrogen (BUN) in control and LPS-treated rats. (**l**) Representative images of H&E staining of renal tissues. n = 4 rats per group. Scale bar = 100 μm. *P < 0.05, **P < 0.01, ****P < 0.0001.

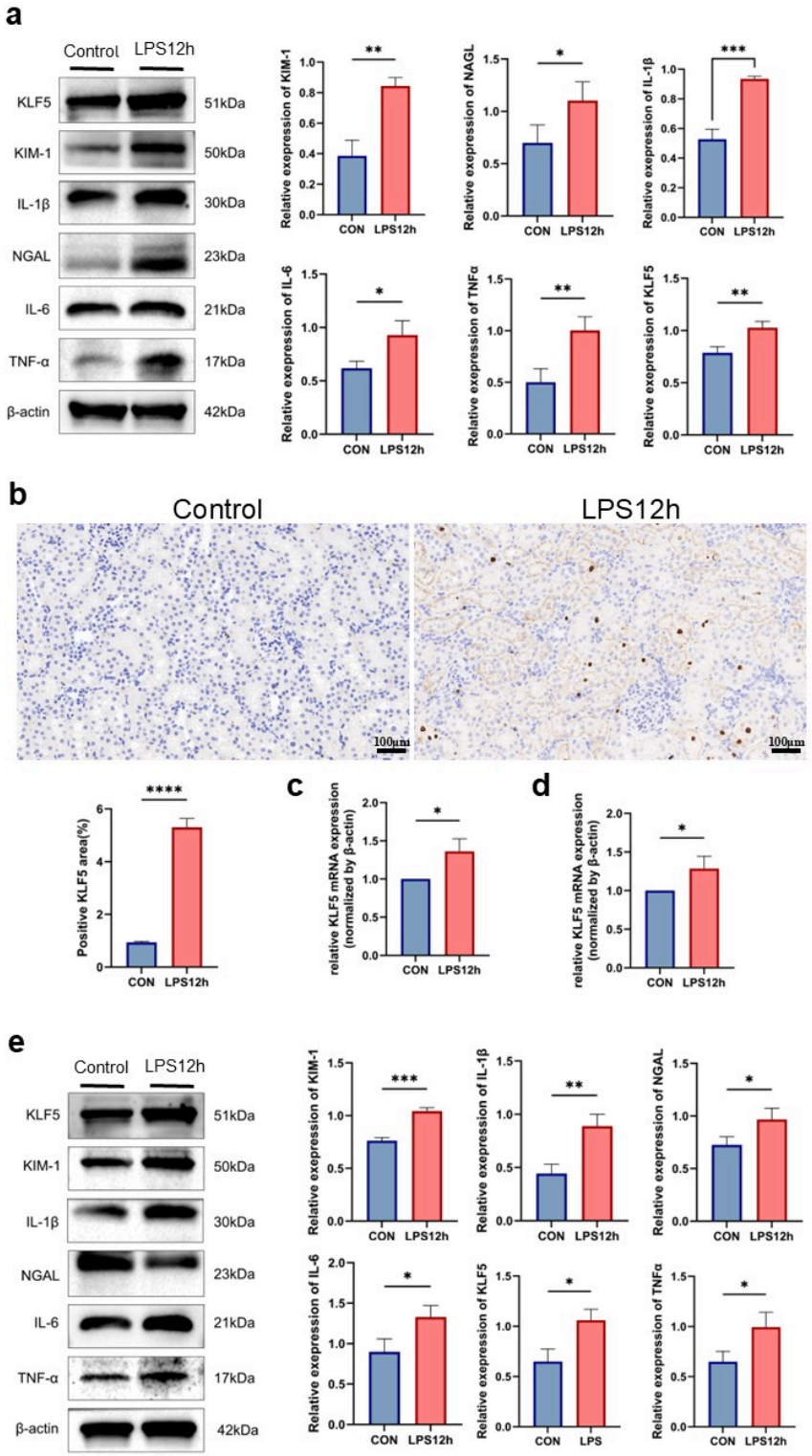


Figure 2

KLF5 expression is elevated in SA-AKI both in vivo and in vitro (**a**) Representative Western blot analysis of KLF5, renal injury and inflammatory markers (KIM-1, NGAL, IL-6, IL-1β, TNF-α) in rat renal tissues. (**b**) Representative images of immunohistochemical staining of KLF5 in rat renal tissues. n = 4 rats per group. Scale bar = 100 μm. (**c**) mRNA levels of KLF5 in rat renal tissues detected by qRT-PCR. (**d**) mRNA levels of KLF5 in HK-2 cells detected by qRT-PCR. (**e**) Representative Western blot analysis of KLF5, renal injury and inflammatory markers (KIM-1, NGAL, IL-6, IL-1β, TNF-α) in HK-2 cells with or without LPS treatment. Data are the mean ± SEM of at least three independent experiments. *P < 0.05, **P < 0.01, ***P < 0.001, ****P < 0.0001

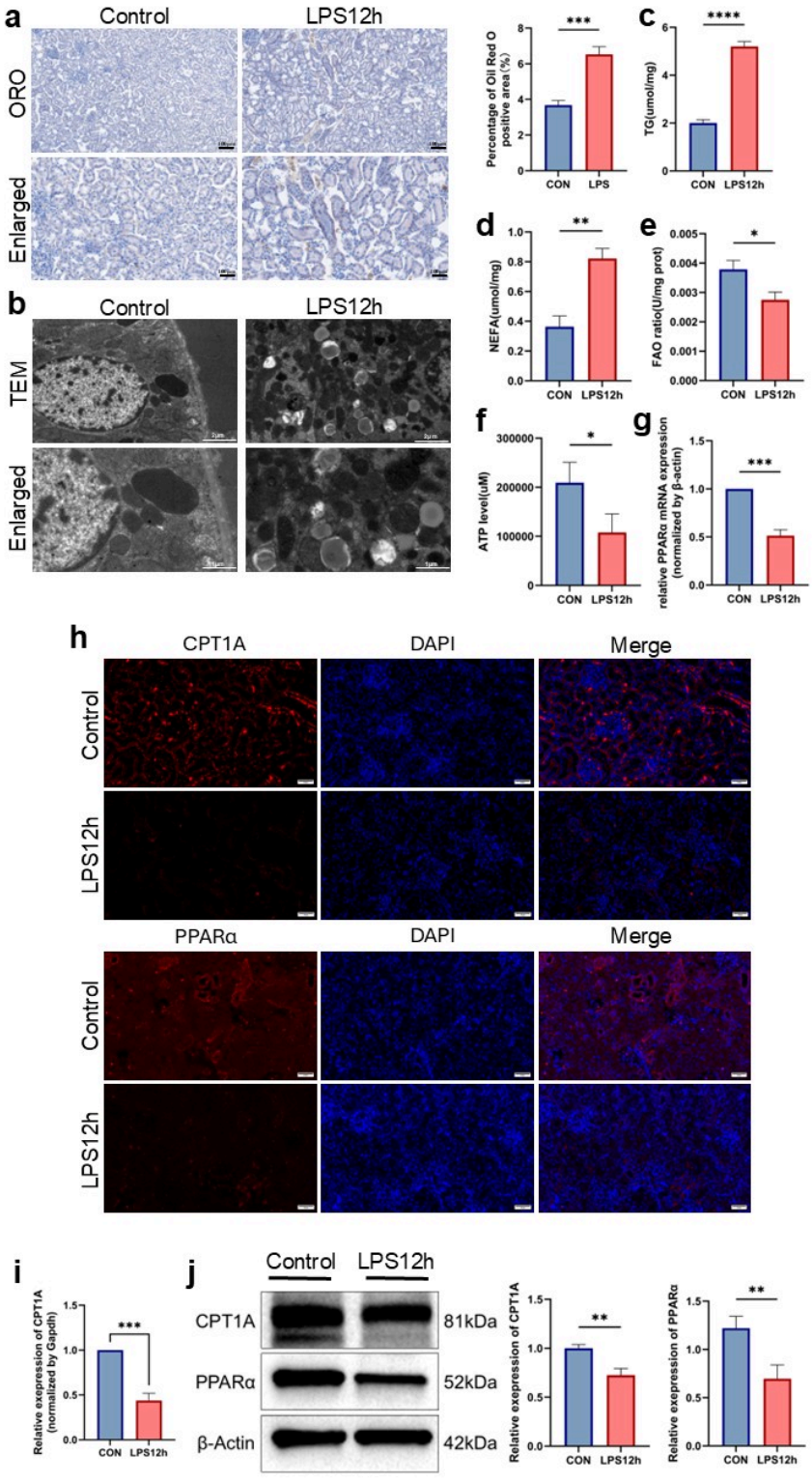


Figure 3

Fatty acid oxidation function is impaired in SA-AKI renal tissues and HK-2 cells (**a**) Representative images of Oil Red O staining of lipid droplets in rat renal tissues. (**b**) Representative TEM images showing mitochondrial and lipid droplet ultrastructure in renal tubular epithelial cells. n = 4 rats per group. (**c**) Levels of triglyceride (TG) in rat renal tissues. (**d**) Levels of non-esterified fatty acid (NEFA) in rat renal tissues. (**e**) FAO rate in rat renal tissues. (**f**) ATP content in rat renal tissues. (**g**) mRNA levels of

PPARA in rat renal tissues. (**h**) Representative images of immunofluorescence staining of CPT1A and PPARα in rat renal tissues. n = 4 rats per group. Scale bar = 100 μm. (**i**) mRNA levels of *CPT1A* in rat renal tissues. (**j**) Protein levels of PPARα and CPT1A in rat renal tissues detected by Western blot. Data are the mean ± SEM of at least three independent experiments. *P < 0.05, **P < 0.01, ***P < 0.001, ****P < 0.0001

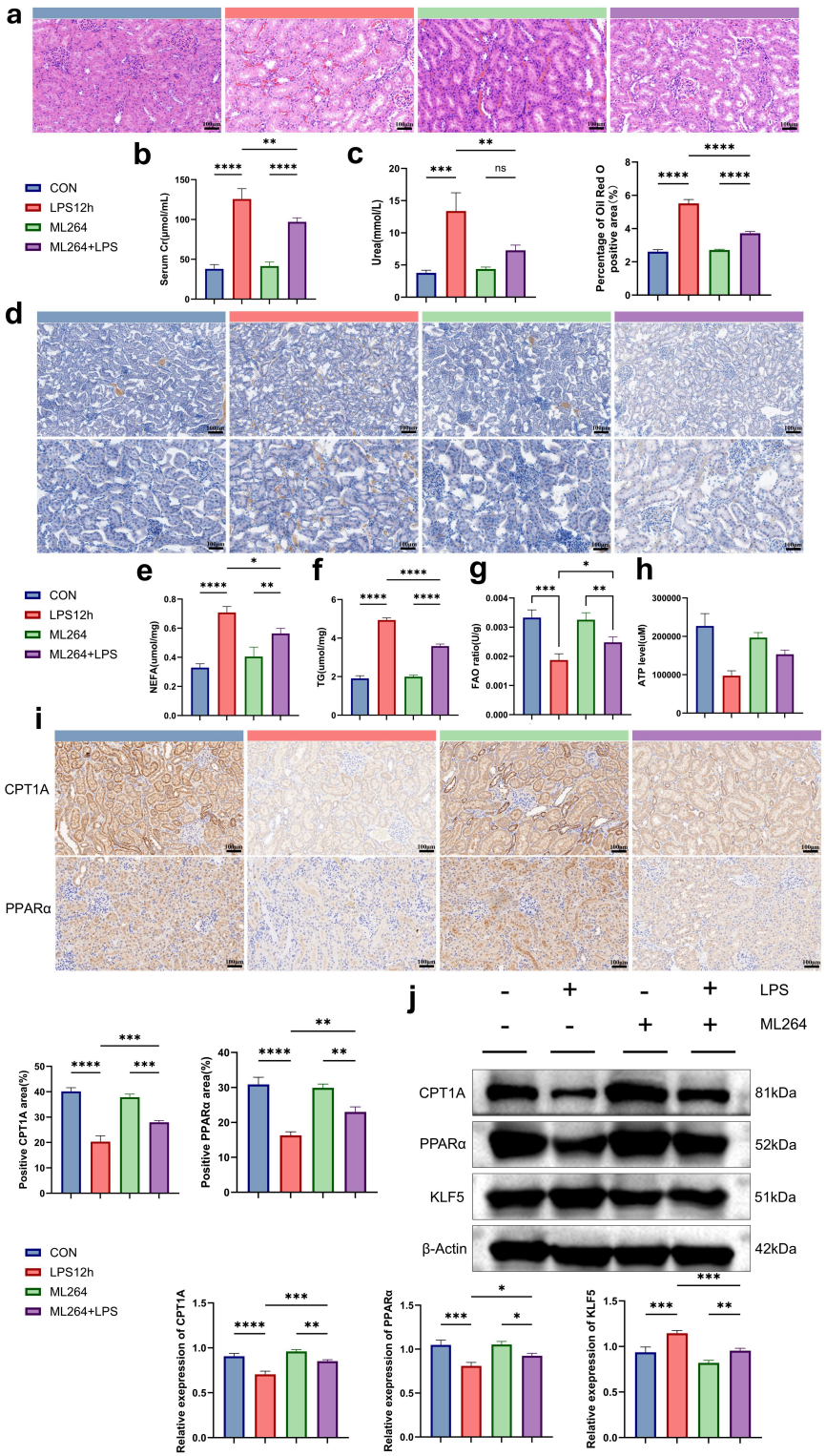


Figure 4

Pharmacological inhibition of KLF5 by ML264 ameliorates renal FAO impairment in SA-AKI rats(**a-c**) Evaluation of renal injury after ML264 treatment: representative H&E staining, serum Scr and BUN levels. (**d-f**) Detection of lipid accumulation after ML264 treatment: representative Oil Red O staining, renal TG and NEFA levels. n = 4 rats per group. Scale bar = 100 μm. (**g-h**)Renal ATP content and FAO rate after ML264 treatment. (**i**). Representative images of immunohistochemical staining of CPT1A and PPARα in rat renal tissues after ML264 treatment. n = 4 rats per group. Scale bar = 100 μm. (**j**) Representative Western blot and quantitation of KLF5, PPARα and CPT1A protein levels in renal tissues. Data are the mean ± SEM of at least three independent experiments. *P < 0.05, **P < 0.01, ***P < 0.001, ****P < 0.0001

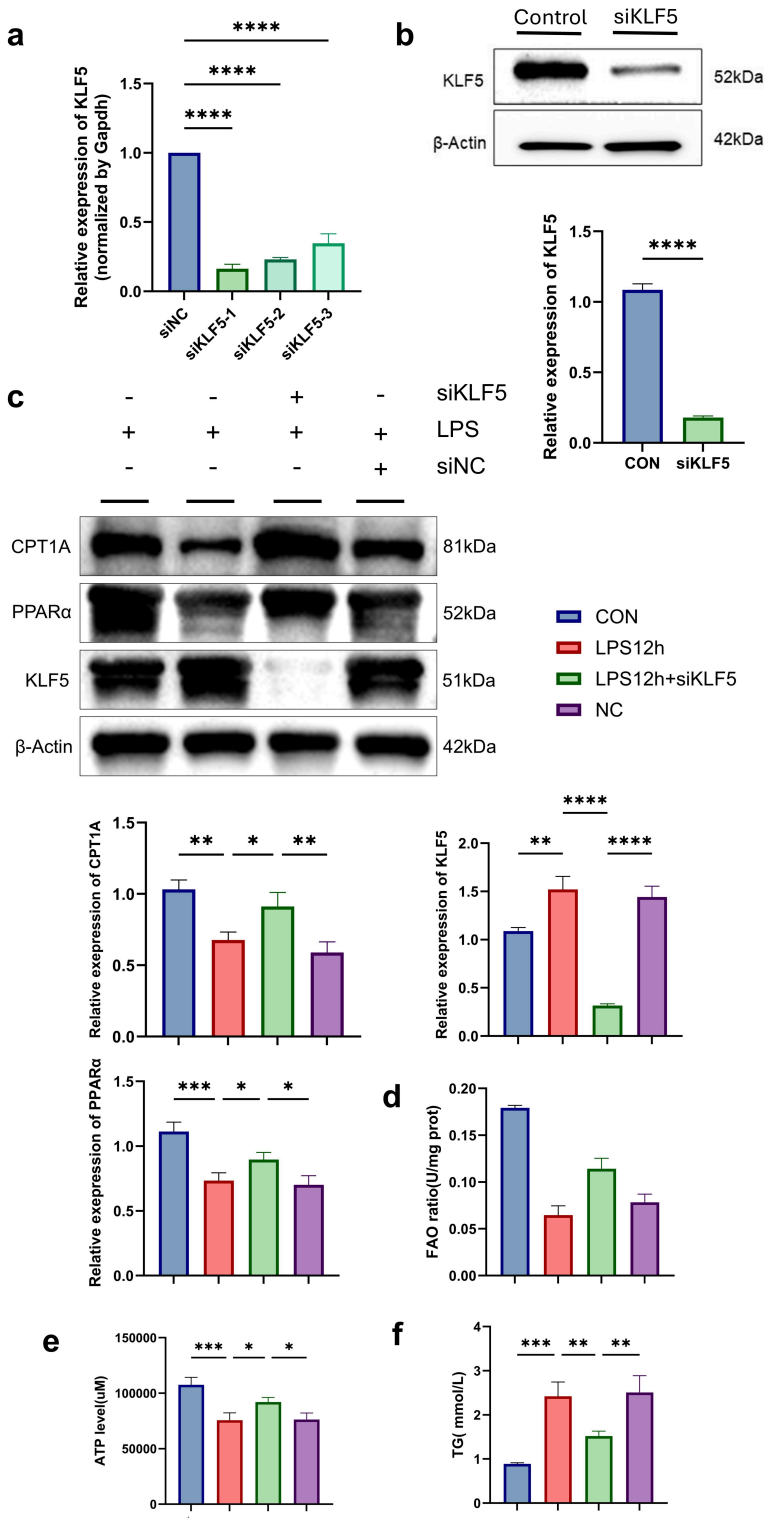


Figure 5

Knockdown of KLF5 alleviates LPS-triggered FAO impairment in HK-2 cells (**a**) Knockdown efficiency of three siKLF5 sequences in HK-2 cells detected by qRT-PCR. (**b**) Protein knockdown efficiency of siKLF5-1 verified by Western blot. (**c**) Protein levels of PPARα and CPT1A in HK-2 cells after KLF5 knockdown, detected by Western blot. (**d-f**) Lipid accumulation, ATP content and FAO rate in HK-2 cells after KLF5

knockdown. Data are the mean ± SEM of at least three independent experiments. *P < 0.05, **P < 0.01, ***P < 0.001, ****P < 0.0001

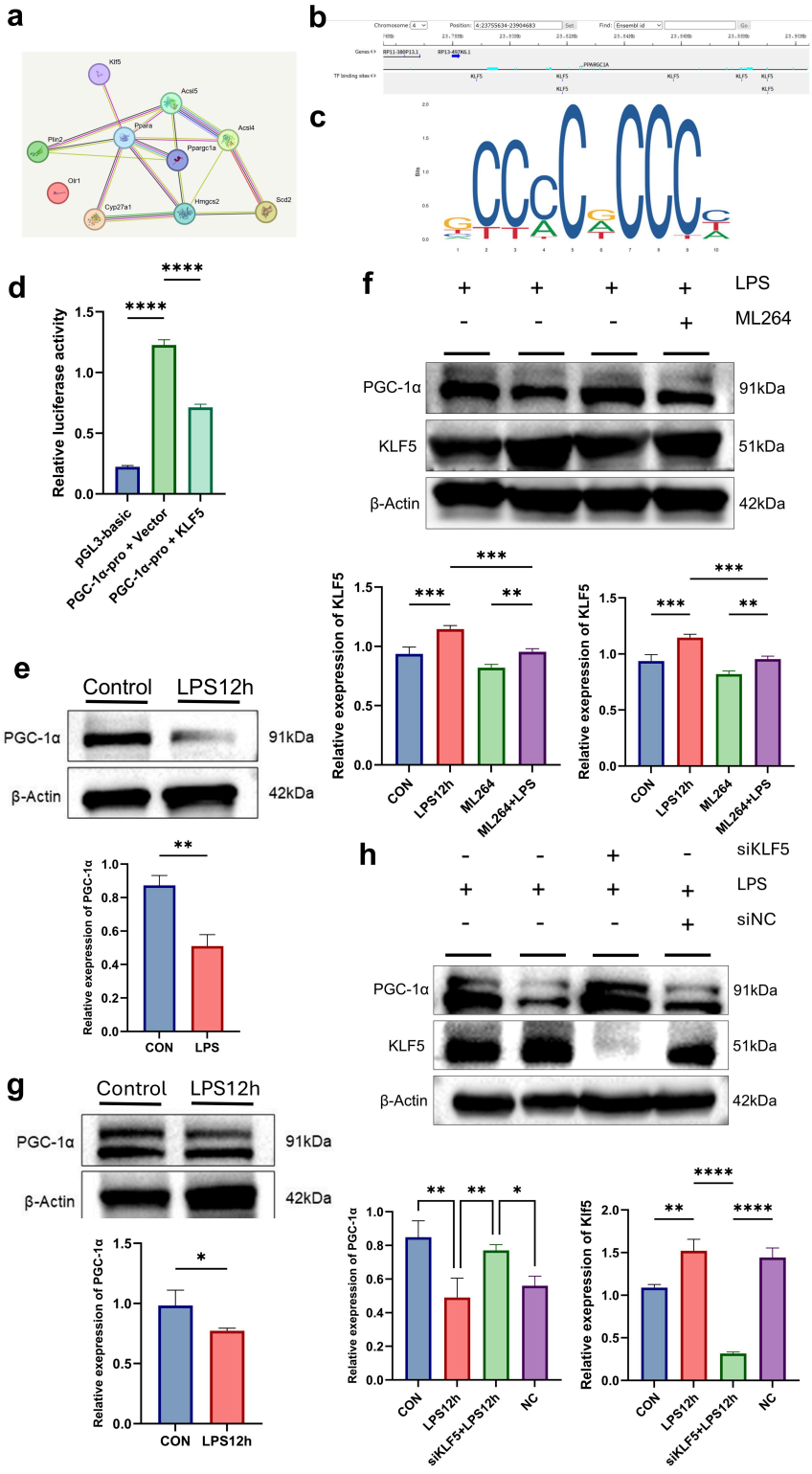


Figure 6

KLF5 transcriptionally downregulates PGC-1α expression during SA-AKI (**a**) Protein-protein interaction prediction between KLF5 and PGC-1α via STRING database. (**b**) Binding peaks of KLF5 in the *PPARGC1A*

promoter region from GTRD database. (**c**) JASPAR database analysis showing the conserved KLF5 binding motif identified in the *PPARGC1A* promoter region. (**d**) Dual-luciferase reporter assay for the regulatory effect of KLF5 on *PPARGC1A* promoter activity. (**e-f**) Protein levels of PGC-1α in rat renal tissues with or without LPS/ML264 treatment. n = 4 rats per group. (**g-h**) mRNA and protein levels of PGC-1α in HK-2 cells with or without LPS/siKLF5 treatment. Data are the mean ± SEM of at least three independent experiments. *P < 0.05, **P < 0.01, ***P < 0.001, ****P < 0.0001.

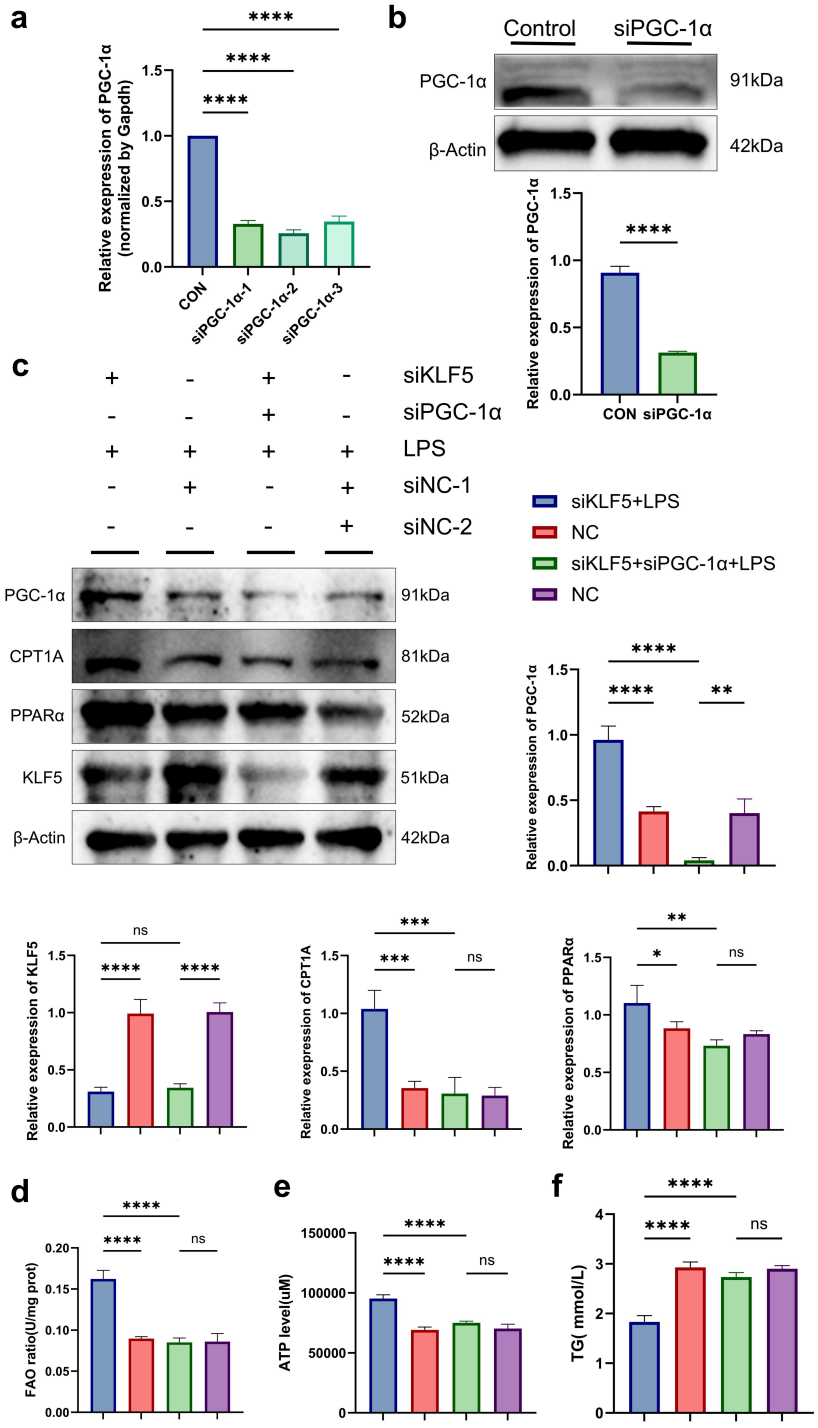


Figure 7

PGC-1α knockdown abolishes the protective effects of KLF5 inhibition on FAO function (**a-b**) Knockdown efficiency of three siPGC-1α sequences in HK-2 cells detected by qRT-PCR and Western blot. (**c**) Protein levels of PPARα and CPT1A in the rescue experiment detected by Western blot. (**d-f**). ATP content, FAO rate and TG content in HK-2 cells in the rescue experiment. Data are the mean ± SEM of at least three independent experiments. *P < 0.05, **P < 0.01, ***P < 0.001, ****P < 0.0001.

Supplementary Files

This is a list of supplementary files associated with this preprint. Click to download.

- SupplementaryTableS1.docx
- SupplementaryTableS2.docx
- Supplementaryfile.docx